The Smallest Anions, Induced Porosity and Graphene Interfaces in C12A7:e⁻ Electrides: A Paradigm Shift in Electromagnetic Absorbers and Shielding Materials

Vidhya Lalan[a], Subodh Ganesanpotti[*a]

[a] Department of Physics, University of Kerala, Thiruvananthapuram, Kerala, 695581, India

E-mail: gsubodh@gmail.com, gsubodh@keralauniversity.ac.in

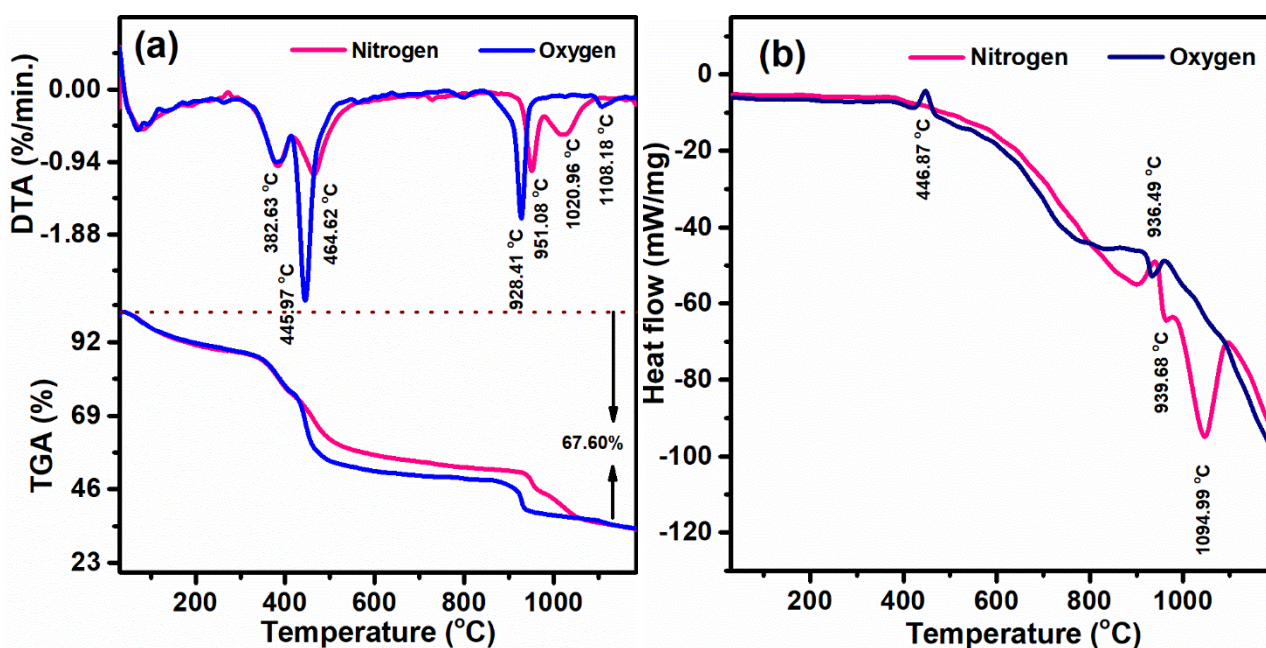**TG-DT and DSC Analysis of the precursor**

Fig. S1 (a) TGA/DTA curves and (b) DSC curve of the sol-gel precursor under N_2 and O_2 environment.

The thermal analysis of the precursor, obtained after the 275°C heat-treatment, was done using TG-DT and DSC analysis under the nitrogen and oxygen atmosphere. The heating rate employed was 5 °Cmin⁻¹, and the corresponding curves are shown in Fig. S1 (a) and (b),

respectively. There are five significant weight changes in the TGA curve, and corresponding peaks were observed in the DTA curve. The evaporation of adsorbed water molecules and ethylene glycol decomposition were observed near 100 and 382 °C, respectively. Decomposition of metal nitrates and the formation of their corresponding oxides usually occur around 450 °C.[1] Two primary phase decomposition occurs 900 and 1000 °C, indicating the formation of intermediate phases other than C12A7 from CaO and Al_2O_3 phases. The complete formation of the mayenite phase occurs after the decomposition beyond 1000 °C. The total weight loss observed after the completion of the reaction at 1200 °C is 67.60%. In the DSC analysis, there is an exothermic peak at 446 °C in the presence of oxygen, which indicates the possible oxidation of carbon atoms that remained in the material after the decomposition of ethylene glycol. Beyond that temperature, the reaction involves the endothermic processes of the decomposition of $Al(NO_3)_3$ to Al_2O_3 and nitrous oxide.[2] The decomposition of $Ca(NO_3)_2$ into CaO, nitrous oxide, and O_2 takes place around 561 °C.[3] The decompositions of intermediate phases around 900 and 1000 °C were endothermic, both in oxygen and nitrogen environment.

UV-Visible Spectroscopy

The UV-Visible spectra of C12A7 and C12A7:e⁻ are shown in Fig. S2c. The band structure of C12A7 consists of a conduction band and valence band called framework-conduction-band (FCB) and framework-valence-band (FVB). A significant level of empty cages forms a cage conduction band (CCB) which is 2 eV below FCB, and the trapped O^{2-} ions in the cages forms energy level which is 1 eV above the FVB[4]. Here, the 4.5 eV absorption band of pristine C12A7 is due to the transition of electrons from the cage-trapped O^{2-} to the CCB and the absorption above 5.5 eV, indicating the transition from FVB to FCB[5]. The reduction shifts the absorption to the lower energy side. The lower energy absorption arises from two types of electron transitions, the first is due to the intra-cage electron transition to a 1p excited-state in the same cage, and the other is due to the inter-cage transition of electrons from the 1s level of occupied cages to the 1s level of empty cages[6]. The observed shift in absorption energy indicates the replacement of O^{2-} ions with electrons in C12A7:e⁻.
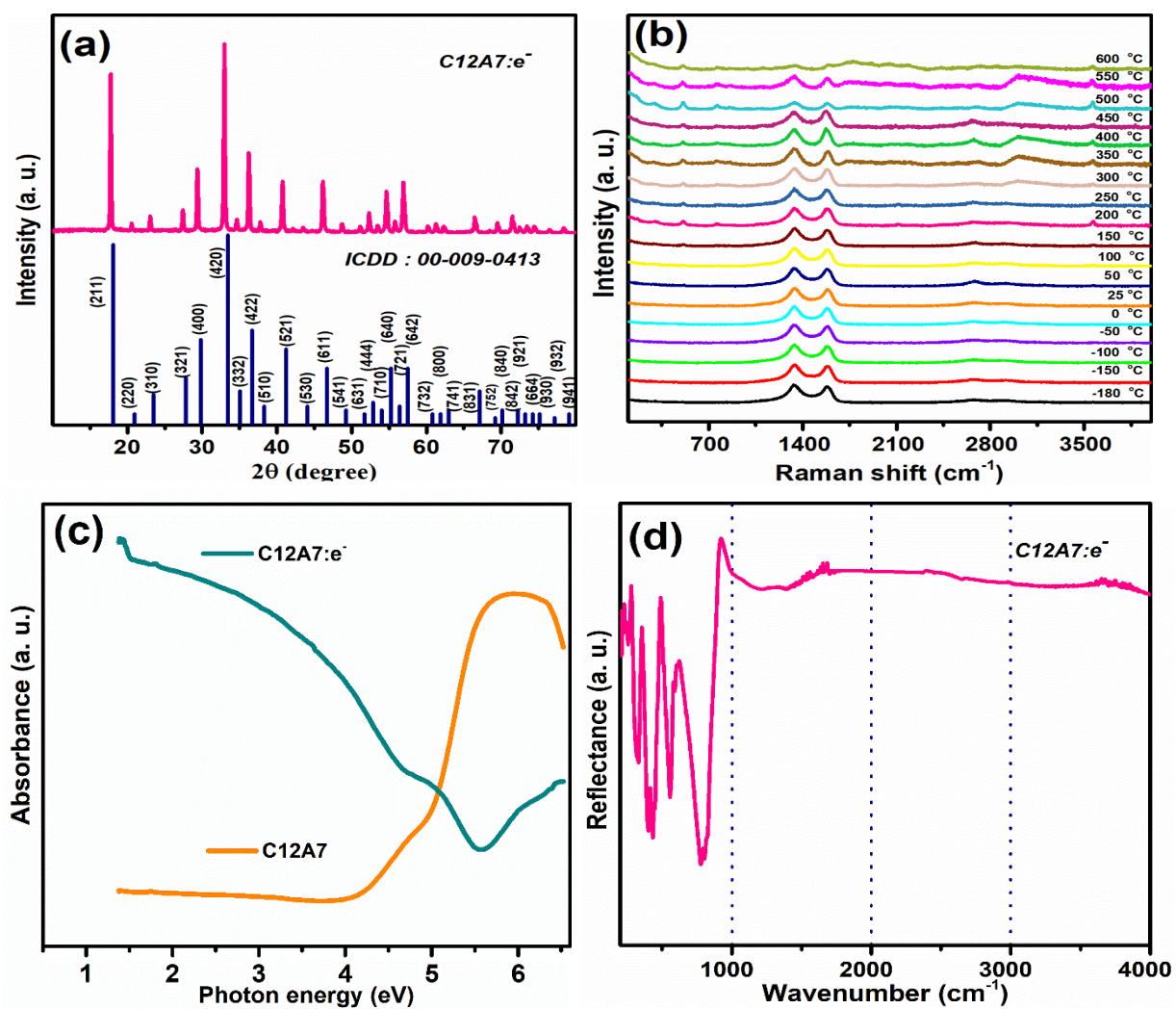
Fig. S2 (a) XRD pattern, (b) temperature-dependent Raman spectra, (c) UV-Visible absorption spectra and (d) FTIR spectra from 200 to 4000 cm^{-1}.
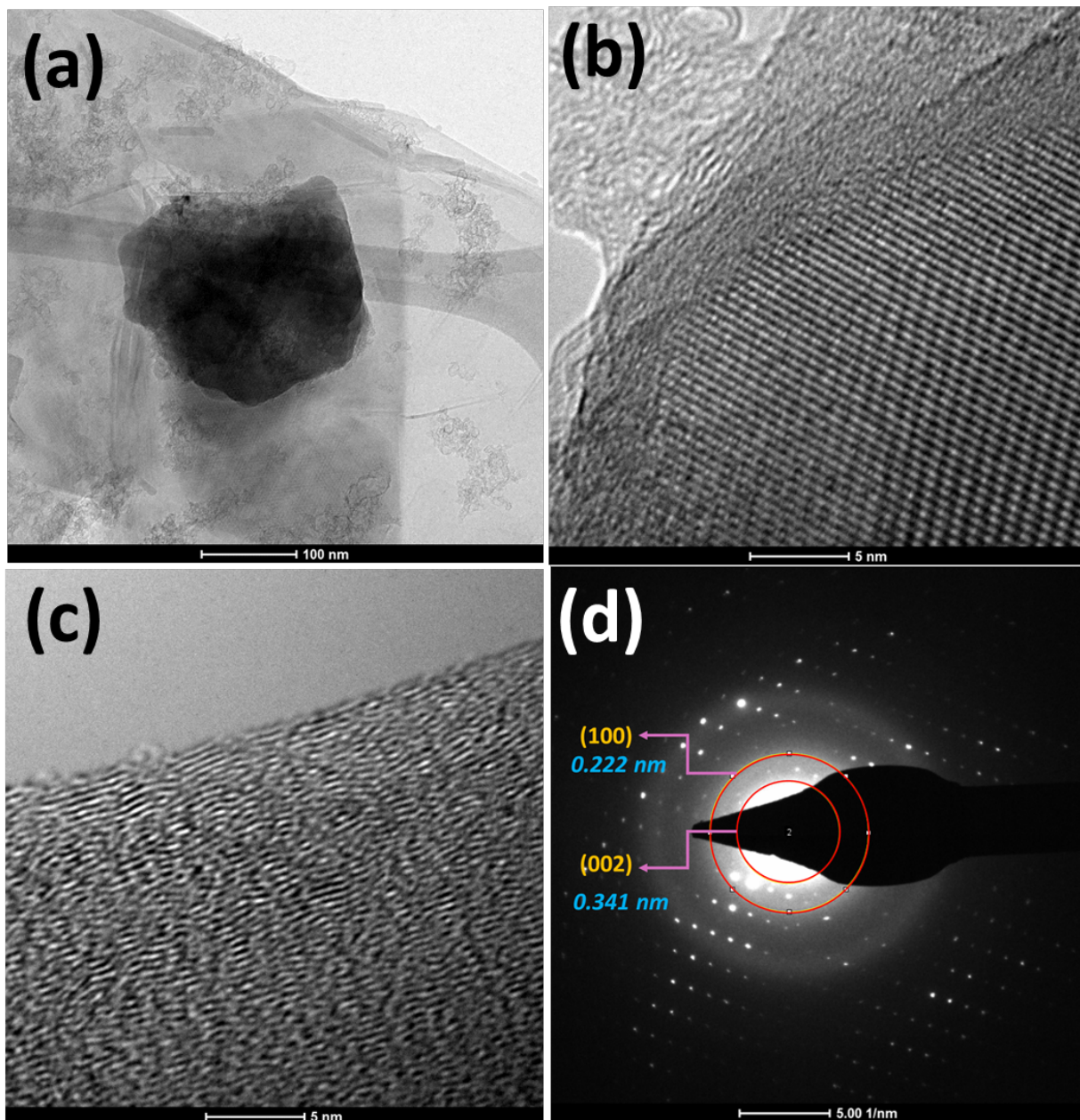
Fig. S3 (a, b, c) HRTEM images from the MG/C12A7:e⁻ interfaces and (b) SEAD pattern.
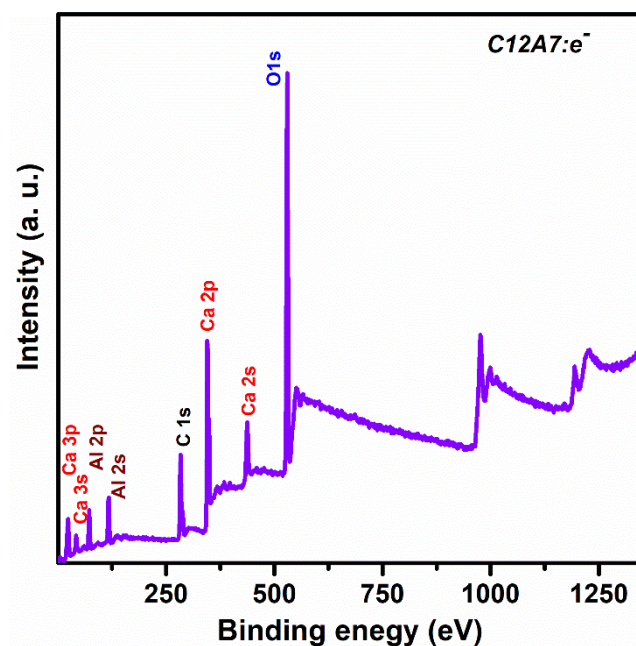
Fig. S4 XPS survey spectra of C12A7:e⁻.

Table S1**.** XPS peak assignment and elemental compositions in C12A7:e⁻.

Element	Binding energy [eV]	Peak assignment	FWHM [eV]	Peak Area [cps. eV]	Atomic percentage [%]
	283.0	C-V	1.2	2943.9	9.94
	284.6	C=C/C-C	1.91	16973.5	57.29
C 1s	286.1	C-OH/C-O-C	2.12	3560.4	12.02
	288.6	C=O	2.32	2546.0	8.59
	289.6	O-C=O	1.79	3602.9	12.16
	530.2	C=O	1.96	59384.1	39.28
O 1s	531.6	NBO	2.02	59257.1	39.19
	532.6	BO	2.75	32556.1	21.53
Ca 2p	346.8	Ca-O (2 $p_{3/2}$)	1.88	51172.0	66.90

	350.3	Ca-O ($2p_{1/2}$)	1.98	25321.4	33.10
Al 2p	73.1	Al-O ($2p_{3/2}$)	1.59	6465.2	64.44
	73.9		2.17	3568.1	35.56

Table S2. RC fit parameters of the complex impedance spectra.

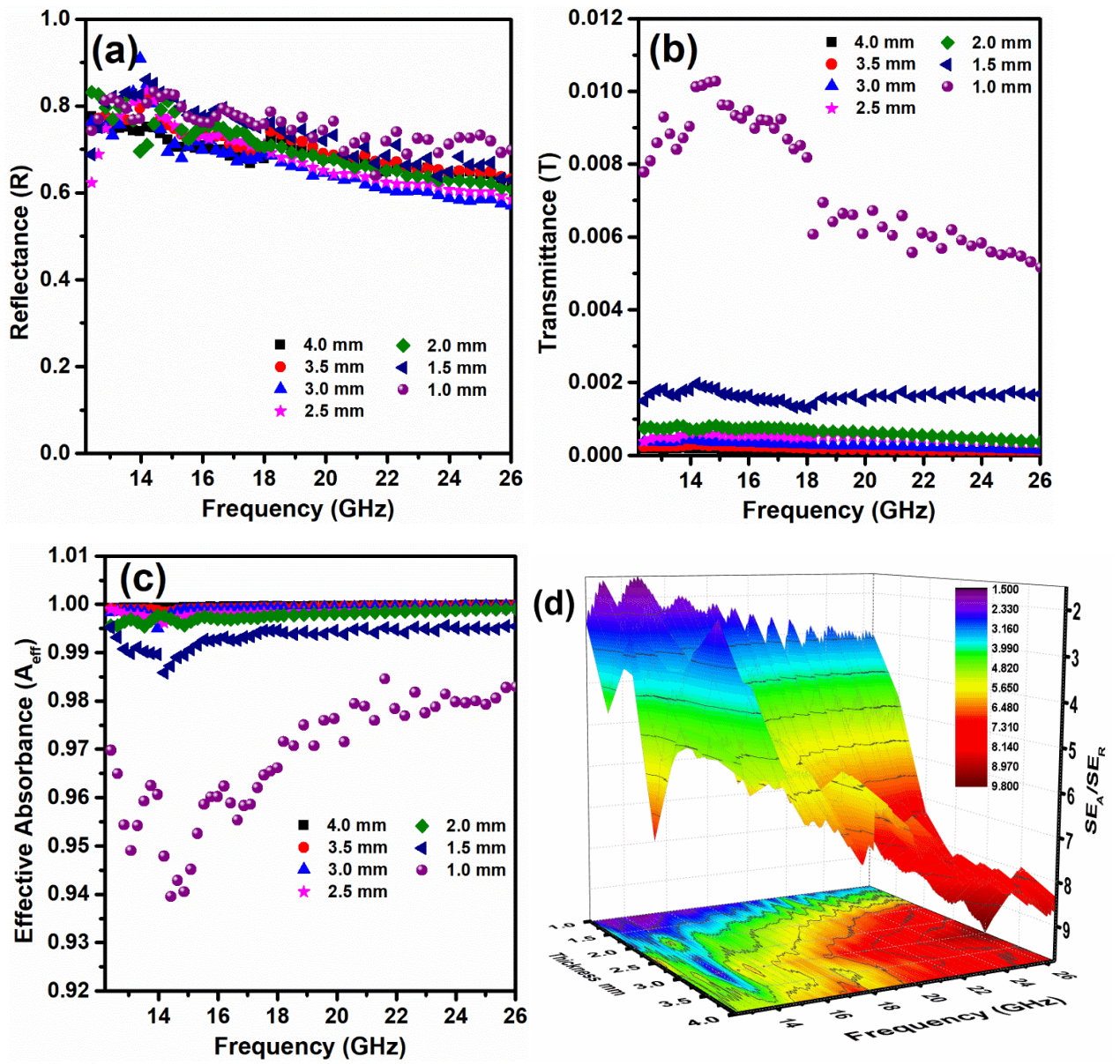| Temperature [K]	R_{gb} [Ω]	C_{gb} [F]	R_g [Ω]	C_g [F]
303	12.3	1.96×10^{-11}	4.7	6.02×10^{-12}
308	11.8	1.97×10^{-11}	4.71	5.82×10^{-12}
313	11.4	1.98×10^{-11}	4.73	5.65×10^{-12}
318	11.1	$2.00E \times 10^{-11}$	4.79	5.64×10^{-12}
323	10.7	$2.02E \times 10^{-11}$	4.84	5.59×10^{-12}
328	10.4	2.04×10^{-11}	4.86	5.46×10^{-12}
338	9.9	2.07×10^{-11}	4.9	5.21×10^{-12}
343	9.65	2.09×10^{-11}	4.94	5.10×10^{-12}

Fig. S5 (a) Reflectance, (b) transmittance, (c) effective absorbance and (d) SE_A/SE_R ration of C12A7:e⁻ pellets.

Table S3. Comparison of EMI SE and SSE of C12A7:e⁻ with other ceramic materials.

Matrix	Filler & Loading	Thickness [mm]	Frequency [GHz]	EMI SE [dB]	SSE [dBcm²g⁻¹]	Ref.
B₄C	GNPs (2 Vol%)	1.5	X	40	103	7

Gd@MoS$_2$	20% Gd +rGO	1.1	X	20.47	-	8
MoS$_2$-rGO	Fe$_3$O$_4$	-	X	8.27	-	9
Si$_3$N$_4$	-	1.5	X	6		10
Si$_3$N$_4$	CNTs (2.7 wt%)	1.5	X	30.4	-	10
Si$_3$N$_4$	PyC (12 vol%)	2.8	X	43.2	76	11
Si$_3$N$_4$	PyC (16.33 wt%) + CNTs (2.94wt%)+ Ni (0.43 wt%)	2	X	43.6	126	12
Si$_3$N$_4$	PyC (4vol%)	2	X	13.5	25	13
Si$_3$N$_4$	SiC (11 vol%)	2.8	X	27		14
SiC	YSZ (2.1 wt%)	5	X	16.2	15	15
SiC	Cf (40 vo%)	3	X	31	50	16
SiC$_f$/SiC	Ti$_3$SiC$_2$ (14.4 wt%)	3	X	20	30	17
SiC$_f$/SiC	PyC (3.3 vol%)	2	X	26	-	18
SiO$_2$	rGO (20 wt%)	1.5	X	36	-	19
SiO$_2$	MWCNTs (10 wt%)	2.5	X	21	-	20
SiO$_2$	C$_f$ (20 wt%)	2.5	X	12	-	21
SiO$_2$	CNTS (10 vol%)	5	X	33	-	22
SiO$_2$	OMC (10 vol%)	5	X	40	-	23
Al$_2$O$_3$	GNP (2 vol%)	1.5	X	23	-	24
Al$_2$O$_3$	Ti$_3$SiC$_2$ (25 vol%)	1	Ku	32	-	25
BaTiO$_3$	GNP (4 wt%)	1.5	X	42	-	26
La$_{0.7}$Sr$_{0.3}$MnO$_3$	-	2	X	19	28	27
Ti$_3$AlC$_2$	-	1.5	X	34		17
Cement-based Ceramics	MnO$_2$ (10 wt%)	2	X	8	20	28

Portland Cement	MWCNTs (15 wt%)	2	X	27	-	29
C12A7: e⁻	-	1		21.6		
		1.5		27.9		
		2		32.3		
		2.5	Ku, K	32.8	107	This work
		3		35.9		
		3.5		38.1		
		4		39.3		

Table S4. Comparison of reflection loss of C12A7:e⁻ with ceramic/conducting/magnetic materials.

Filler	Matrix	Thickness [mm]	RL [dB]	f_m [GHz]	Bandwidth [GHz]	Frequency [GHz]	Ref.
201[a)]-MoS_2-Ni-CNTS (20 wt%)	wax	2.5	-6.68	-	-	2-18	30
201-MoS_2-Ni-CNTS (30 wt%)	wax	2.4	-50.08	11.92	6.04	2-18	30
201-MoS_2-Ni-CNTS (40 wt%)	wax	1.5	-14.84	12.56-17.96	5.40	2-18	30
Ni-MoS_2 (30 wt%)	wax	1.6	-25.19	13.80-18.0	4.2	2-18	30
MoS_2 (60 wt%)	wax	2.4	-38	9.6-13.76		2-18	31
Ni-Al_2O_3-Ni film	wax	3.5	-45.3	11.4	7.1	2-18	32
SiC (50 wt%)+ CB (5 wt%)	wax	2	-41	9	6	2-18	33
Zn Ferrite (50 wt%)	PPy	2.7	-29	10.8	4.2	2-18	34
Mn Ferrite (15 wt%)	PPy	1.5	-12	11.3	-	8-12	35
$Sm_{1.5}Y_{0.5}Fe_{17-x}Si_x$ (3:1)	wax	1	-55.1	14.4	3.7	2-18	36

Gd(OH)$_3$@PPy (20 wt%)	wax	2.2	-51.4	16.2	4.8	2-18	37
Co/Porous carbon (25 wt%)	wax	3	-30.31	11.03	4.93	2-18	38
CNTs derived fom DCDA[b] (2.5 g)	CF[c]	1.6	-42	-	5.08	2-18	39
C12A7: e$^-$(0.4:1)	wax	2.54	-22.9	30.9	10.1		This work
		3.02	-27.1	25.4	9.1	5-40	
		4.24	-43.9	19.1	7.0		

a) 2-dimensional, 0-dimensional, 1-dimensional; b) dicyandiamide; c) carbon fiber

Reference

1   S. N. Ude, C. J. Rawn, R. A. Peascoe, M. J. Kirkham, G. L. Jones and E. Andrew Payzant, *Ceram. Int.*, 2014, **40**, 1117–1123.

2   S. Yuvaraj, F. Y. Lin, T. H. Chang and C. T. Yeh, *J. Phys. Chem. B*, 2003, **107**, 1044–1047.

3   C. Ettarh and A. K. Galwey, *Thermochim. Acta*, 1995, **261**, 125–139.

4   K. Khan, A. K. Tareen, M. Aslam, K. H. Thebo, U. Khan, R. Wang, S. S. Shams, Z. Han and Z. Ouyang, *Prog. Solid State Chem.*, 2019, **54**, 1–19.

5   C. Rudradawong, M. Kitiwan, T. Goto and C. Ruttanapun, *Mater. Today Commun.*, 2020, **22**, 100820.

6   W. Zou, K. Khan, X. Zhao, C. Zhu, J. Huang, J. Li, Y. Yang and W. Song, *Mater. Res. Express*, 2017, **4**, 036408.

7   Y. Q. Tan, H. Luo, X. S. Zhou, S. M. Peng and H. B. Zhang, *RSC Adv.*, 2018, **8**, 39314–39320.

8   J. Prasad, A. K. Singh, K. K. Haldar, V. Gupta and K. Singh, *J. Alloys Compd.*, 2019, **788**, 861–872.

9   J. Prasad, A. K. Singh, J. Shah, R. K. Kotnala and K. Singh, *Mater. Res. Express*, 2018, **5**, 055028.

10   M. Chen, X. Yin, M. Li, L. Chen, L. Cheng and L. Zhang, *Ceram. Int.*, 2015, **41**, 2467–2475.

11   X. Li, L. Zhang and X. Yin, *J. Eur. Ceram. Soc.*, 2013, **33**, 647–651.

12   X. Liu, X. Yin, G. Zheng, Y. Liu, L. Kong, Q. Li and X. Yuan, *Ceram. Int.*, 2014, **40**, 531–540.

13   X. Hao, X. Yin, L. Zhang and L. Cheng, *J. Mater. Sci. Technol.*, 2013, **29**, 249–254.

14   R. D. Veltri and F. S. Galasso, *J. Am. Ceram. Soc.*, 1990, **73**, 2137–2140.

15   X. Yin, Y. Xue, L. Zhang and L. Cheng, *Ceram. Int.*, 2012, **38**, 2421–2427.

16   L. Chen, X. Yin, X. Fan, M. Chen, X. Ma, L. Cheng and L. Zhang, *Carbon*, 2015, **95**, 10–19.

17   Y. Mu, W. Zhou, F. Wan, D. Ding, Y. Hu and F. Luo, *Compos. Part A Appl. Sci. Manuf.*, 2015, **77**, 195–203.

18   D. Ding, Y. Shi, Z. Wu, W. Zhou, F. Luo and J. Chen, *Carbon*, 2013, **60**, 552–555.

19   B. Wen, M. Cao, M. Lu, W. Cao, H. Shi, J. Liu, X. Wang, H. Jin, X. Fang, W. Wang and J. Yuan, *Adv. Mater.*, 2014, **26**, 3484–3489.

20   B. Wen, M. S. Cao, Z. L. Hou, W. L. Song, L. Zhang, M. M. Lu, H. B. Jin, X. Y. Fang, W. Z. Wang and J. Yuan, *Carbon*, 2013, **65**, 124–139.

21   M. S. Cao, W. L. Song, Z. L. Hou, B. Wen and J. Yuan, *Carbon*, 2010, **48**, 788–796.

22   C. Xiang, Y. Pan, X. Liu, X. Sun, X. Shi and J. Guo, *Appl. Phys. Lett.*, 2005, **87**, 1–3.

23   J. Wang, C. Xiang, Q. Liu, Y. Pan and J. Guo, *Adv. Funct. Mater.*, 2008, **18**, 2995–3002.

24   Q. Yuchang, W. Qinlong, L. Fa and Z. Wancheng, *J. Mater. Chem. C*, 2016, **4**, 4853–4862.

25   S. Shi, L. Zhang and J. Li, *J. Appl. Phys.*, 2008, **103**, 124103.

26   Q. Yuchang, W. Qinlong, L. Fa, Z. Wancheng and Z. Dongmei, *J. Mater. Chem. C*, 2016, **4**, 371–375.

27   H. A. Reshi, A. P. Singh, S. Pillai, R. S. Yadav, S. K. Dhawan and V. Shelke, *J. Mater. Chem. C*, 2015, **3**, 820–827.

28   S. D. Hutagalung, N. H. Sahrol, Z. A. Ahmad, M. F. Ain and M. Othman, *Ceram. Int.*, 2012, **38**, 671–678.

29   A. P. Singh, B. K. Gupta, M. Mishra, Govind, A. Chandra, R. B. Mathur and S. K. Dhawan, *Carbon*, 2013, **56**, 86–96.

30   Y. Sun, J. Xu, W. Qiao, X. Xu, W. Zhang, K. Zhang, X. Zhang, X. Chen, W. Zhong and Y. Du, *ACS Appl. Mater. Interfaces*, 2016, **8**, 31878–31886.

31   M. Q. Ning, M. M. Lu, J. B. Li, Z. Chen, Y. K. Dou, C. Z. Wang, F. Rehman, M. S. Cao and H. B. Jin, *Nanoscale*, 2015, **7**, 15734–15740.

32   H. Wei, L. Cheng and D. Shchukin, *Materials (Basel).*, 2020, **13**, 1764.

33   X. Liu, Z. Zhang and Y. Wu, *Compos. Part B Eng.*, 2011, **42**, 326–329.

34   Y. Li, R. Yi, A. Yan, L. Deng, K. Zhou and X. Liu, *Solid State Sci.*, 2009, **11**, 1319–1324.

35   S. H. Hosseini and A. Asadnia, *J. Nanomater.*, 2012, **2012**, 1-6.

36   W. Yang, Y. Zhang, G. Qiao, Y. Lai, S. Liu, C. Wang, J. Han, H. Du, Y. Zhang, Y.

Yang, Y. Hou and J. Yang, *Acta Mater.*, 2018, **145**, 331–336.

37   W. Wei, X. Liu, W. Lu, H. Zhang, J. He, H. Wang and Y. Hou, *ACS Appl. Mater. Interfaces*, 2019, **11**, 12752–12760.

38   H. Wang, L. Xiang, W. Wei, J. An, J. He, C. Gong and Y. Hou, *ACS Appl. Mater. Interfaces*, 2017, **9**, 42102–42110.

39   Y. Cheng, H. Zhao, H. Lv, T. Shi, G. Ji and Y. Hou, *Adv. Electron. Mater.*, 2020, **6**, 1900796.